# Current Biology

# Defining the Substrate Spectrum of the TIM22 Complex Identifies Pyruvate Carrier Subunits as Unconventional Cargos

## Highlights

- Substrates of mitochondrial TIM22 complex identified by proteomics in *S. cerevisiae*

- Carrier proteins with six membrane spans confirmed as substrates

- Pyruvate carrier (MPC) subunits (two or three membrane spans) transported by TIM22

- MPC import dependence on TIM22 is conserved from yeast to human

## Authors

Ridhima Gomkale,
Luis Daniel Cruz-Zaragoza,
Ida Suppanz, ..., David Pacheu-Grau,
Bettina Warscheid, Peter Rehling

## Correspondence

peter.rehling@medizin.uni-goettingen.de

## In Brief

Mitochondria carrier proteins, which possess six transmembrane spans (TM), are transported by the TIM22 complex. By using a quantitative proteomic approach, Gomkale and Cruz-Zaragoza et al. reveal subunits of the mitochondrial pyruvate carrier (MPC) that possess two or three TMs as unexpected substrates of the carrier pathway.

CellPress

# Defining the Substrate Spectrum of the TIM22 Complex Identifies Pyruvate Carrier Subunits as Unconventional Cargos

Ridhima Gomkale,[1,7] Luis Daniel Cruz-Zaragoza,[1,7] Ida Suppanz,[2,3] Bernard Guiard,[4] Julio Montoya,[5] Sylvie Callegari,[1] David Pacheu-Grau,[1] Bettina Warscheid,[2,3] and Peter Rehling[1,6,8,*]

[1]Department of Cellular Biochemistry, University Medical Center Göttingen, 37073 Göttingen, Germany
[2]Biochemistry and Functional Proteomics, Institute of Biology II, Faculty of Biology, University of Freiburg, 79104 Freiburg, Germany
[3]Signalling Research Centres BIOSS and CIBSS, University of Freiburg, 79104 Freiburg, Germany
[4]Centre de Génétique Moléculaire, CNRS, 91190 Gif-sur-Yvette, France
[5]Departamento de Bioquímica y Biología Molecular y Celular, Universidad de Zaragoza-CIBER de Enfermedades Raras (CIBERER)-Instituto de investigación Sanitaria de Aragón (IIS Aragón), 50013 Zaragoza, Spain
[6]Max Planck Institute for Biophysical Chemistry, 37077 Göttingen, Germany
[7]These authors contributed equally
[8]Lead Contact
*Correspondence: peter.rehling@medizin.uni-goettingen.de
https://doi.org/10.1016/j.cub.2020.01.024

## SUMMARY

In mitochondria, the carrier translocase (TIM22 complex) facilitates membrane insertion of multi-spanning proteins with internal targeting signals into the inner membrane [1–3]. Tom70, a subunit of TOM complex, represents the major receptor for these precursors [2, 4–6]. After transport across the outer membrane, the hydrophobic carriers engage with the small TIM protein complex composed of Tim9 and Tim10 for transport across the intermembrane space (IMS) toward the TIM22 complex [7–12]. Tim22 represents the pore-forming core unit of the complex [13, 14]. Only a small subset of TIM22 cargo molecules, containing four or six transmembrane spans, have been experimentally defined. Here, we used a *tim22* temperature-conditional mutant to define the TIM22 substrate spectrum. Along with carrier-like cargo proteins, we identified subunits of the mitochondrial pyruvate carrier (MPC) as unconventional TIM22 cargos. MPC proteins represent substrates with atypical topology for this transport pathway. In agreement with this, a patient affected in TIM22 function displays reduced MPC levels. Our findings broaden the repertoire of carrier pathway substrates and challenge current concepts of TIM22-mediated transport processes.

## RESULTS

### Inactivation of TIM22 for Quantitative Proteomic Analyses

Multi-spanning inner mitochondrial membrane (IMM) proteins with internal targeting signals utilize the carrier import pathway (Figure 1A). However, only a few of these cargo molecules have been experimentally defined by *in vitro* import analyses (AAC, Mir1, Tim22, Mrs3, Tim17, Tim23, and DiC) [9, 14–17]. To broaden the substrate spectrum of this pathway, we established a quantitative proteomic approach following the concept of importomics [18] by using a *tim22* temperature-conditional (ts) yeast mutant *tim22-14* [19]. *tim22-14* mitochondria that were shifted to the non-permissive temperature prior to import analyses display assembly defects for the well-defined substrates Mir1 and Tim23 (Figures 1B and 1C). This import defect was also apparent *in vivo*, where an N-terminally GFP-tagged Mir1 mislocalized from mitochondria upon shift of *tim22-14* cells to the non-permissive temperature (Figure S1A). To this end, mitochondria were isolated from wild-type (WT) and *tim22-14* cells after growing them either at 25°C or 37°C. At the non-permissive temperature, *tim22-14* mitochondria displayed reduced levels of Mir1 (36.5% of WT) and Aac2, whereas the mutant Tim22 was undetectable (Figure S1B). Components of other mitochondrial complexes were not significantly affected. Therefore, we subjected *tim22-14* cells to extended growth times (15, 25, and 40 h) at the non-permissive temperature for subsequent proteomic analyses of purified mitochondria. Mitochondria isolated from all eight conditions were analyzed for steady-state protein levels (Figure 1D). As expected, Tim22 was moderately reduced at the 0 h time point in *tim22-14* and could not be detected at longer time points. The carriers Mir1 and Aac2 displayed reduced levels with increasing growth time at the non-permissive temperature (48.8% and 45.7% of WT at 25 h, respectively). However, other substrates of the TIM22 complex, Tim17 and to a lesser extent Tim23 were affected (54.2% and 80.3% of WT at 25 h, respectively). Blue native (BN)-PAGE analyses revealed that the levels of Aac2 and Mir1 were reduced in mitochondria isolated from *tim22-14* cells grown at the non-permissive temperature, whereas complex V was not affected (Figure 1E).

Purified mitochondria isolated under the conditions described above were subjected to differential stable isotope dimethyl-based labeling and mass spectrometric analyses. Under non-permissive conditions, Tim22 was more than ten times less
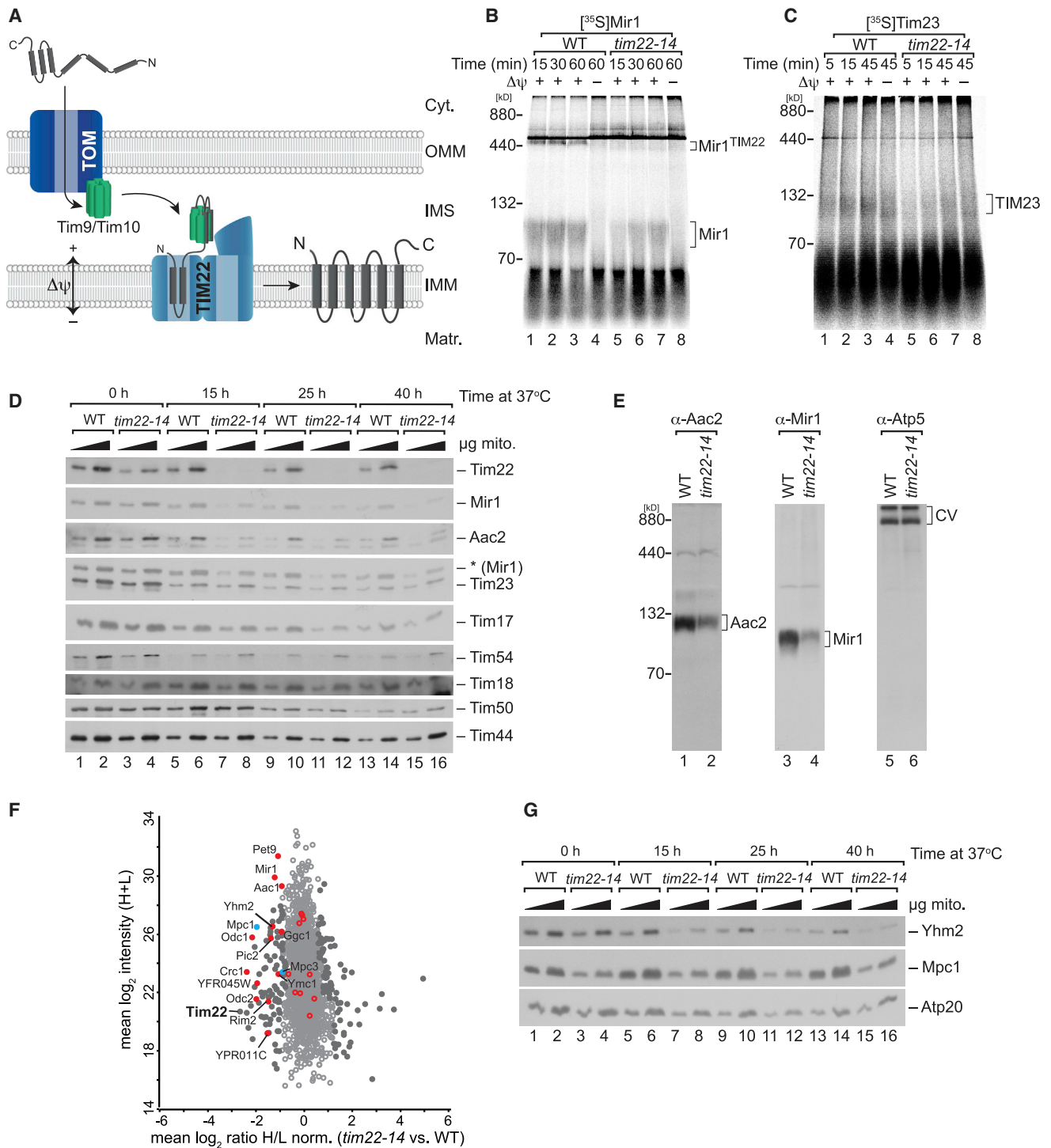
**Figure 1. *tim22-14* Displays Defective Mitochondrial Carrier Protein Import under Non-permissive Conditions**

(A) Hydrophobic proteins with internal signals translocate through the TOM complex. In the IMS, the small TIM complex directs cargo to the TIM22 complex for membrane potential-dependent membrane insertion.

(B and C) [35S]-labeled Mir1 (6TM) (B) and Tim23 (4TM) (C) were imported into wild-type (WT) and *tim22-14* mitochondria. Membrane insertion was monitored by BN-PAGE and digital autoradiography.

(D) Mitochondria from cells grown at the non-permissive temperature for indicated times were analyzed by western blotting.

(E) WT and *tim22-14* mitochondria from cells grown at 37°C for 15 h analyzed by BN-PAGE and immunodecoration.

*(legend continued on next page)*

abundant in *tim22-14* mitochondria than in the WT control. Among the most severely affected proteins were the mitochondrial inner membrane carrier proteins (Figure S1C; Table S1). On average, most of the known carrier proteins were significantly less abundant in *tim22-14* than the WT (Figure 1F), supporting the idea that potential cargo candidates for the TIM22 complex should be reduced. In agreement with the mass spectrometric data, the citrate and oxoglutarate carrier (Yhm2) displayed reduced protein levels in *tim22-14* mitochondria with increasing time at 37°C (Figure 1G). We conclude that the mass-spectrometry-based analyses of *tim22-14* mitochondria enabled us to identify known and new potential substrates of the TIM22 complex.

### Identification of Potential Carrier Cargo Proteins

To confirm that selected putative carrier substrates identified by proteomic analyses depended on the TIM22 pathway, we analyzed the import into purified mitochondria from cells grown at a permissive temperature. To exclude indirect effects of the *tim22* mutant on the presequence pathway, we imported the model matrix proteins Su9-DHFR and Atp5. Both precursors were efficiently imported into WT and *tim22-14* mitochondria after heat shock (Figure S2A). Moreover, imported Atp5 assembled with similar efficiency into the $F_1F_o$-ATP synthase in both strains (Figure S2B).

The import of the carrier proteins Yhm2, Crc1 (carnitine carrier), Odc1 (oxodicarboxylate carrier), and the glycine transporter Hem25 (Heme synthesis by SLC25 family member), which display standard six transmembrane topology, has not been investigated. Since they were identified as candidate cargo proteins, we performed *in vitro* import and assembly assays of [$^{35}$S]-labeled proteins into WT and *tim22-14* mitochondria combined with BN-PAGE analyses. As assessed by western blot and assembly analysis, Yhm2 steady-state levels and import were reduced in *tim22-14* mitochondria (Figures 2A and 2B). Similarly, Crc1, Odc1, and Hem25 assembly were affected in *tim22-14* mitochondria (Figures 2C–2E). To assess dependence on the receptor Tom70 and the small TIM chaperone complex, these proteins were imported into *tim10-2* [10] and *tom70/71ΔΔ* [20] mitochondria. In both cases, reduced assembly was apparent (Figures 2F and S2C). These results confirmed the mass spectrometric data that Yhm2, Crc1, Odc1, and Hem25 are substrates of the carrier transport pathway.

Two uncharacterized mitochondrial proteins, Yfr045w and Ypr011c, displayed reduced levels in *tim22-14* (Figure 1F). *In silico* analyses suggested both proteins as members of the mitochondrial transporter family [21]. However, metazoan homologs were not apparent. Transmembrane domain prediction algorithms suggest that Yfr045w contains six transmembrane spans. In contrast, the same algorithms failed to predict transmembrane domains in Ypr011c. Nevertheless, based on protein alignments with Aac3, six transmembrane segments could be suggested

with a similar topology to Yfr045w (Figure S2D). *yfr045wΔ* and *ypr011cΔ* mutant cells displayed reduced growth on glycerol-containing media in comparison with WT cells (Figure S2E). This suggested that both proteins were required for mitochondrial activity. Recombinantly expressed Ypr011c was suggested to be a mitochondrial transporter for adenosine 5′-phosphosulfate and 3′-phospho-adenosine 5′-phosphosulfate, whereas *in vivo* studies suggested a role in thermotolerance of yeast [22]. When we addressed the import of [$^{35}$S]-labeled Yfr045w and Ypr011c, we found it to be reduced in *tim22-14* and *tim10-2* mutant mitochondria (Figures 2G–2I), indicating that both proteins are inserted into the IMM by the TIM22 complex with contribution of the small Tim proteins.

### Pyruvate Carrier Subunits Are Imported along the Carrier Pathway

The mitochondrial pyruvate carrier (MPC) is a conserved hetero-oligomeric complex that transports pyruvate across the mitochondrial inner membrane [23, 24]. In yeast, depending on the carbon source, the functional complex contains Mpc1-Mpc2 as a "fermentative" complex and Mpc1-Mpc3 as a "respiratory" complex. Mpc1 and Mpc3 levels were reduced in mitochondria upon inactivation of Tim22 (Figures 1F and 1G; Table S1). We confirmed this reduction by BN-PAGE analyses (Figure 3A). A low-molecular-mass Mpc1 form (MPC1*), potentially representing a free Mpc1 pool, was also decreased in mutant mitochondria.

As described above, a hallmark of TIM22-dependent cargo proteins is the even number (four or six) of transmembrane spans with N and the C termini facing the intermembrane space (IMS) [25, 26]. Interestingly, Mpc1 contains two, whereas Mpc2 and Mpc3 contain three putative transmembrane spanning regions (Figure S3A). Mpc1 exposes both N and C termini into the matrix, whereas in the case of Mpc2 and Mpc3 the N and the C terminus are exposed to the matrix and the IMS, respectively [27]. This topology and number of transmembrane spans differ significantly from known TIM22 cargo proteins.

When [$^{35}$S]-labeled Mpc1 was imported into WT mitochondria, it failed to incorporate into the MPC complex. Interestingly, in *mpc1Δ* mitochondria, the imported Mpc1 protein assembled efficiently into the MPC complex (Figure 3B). This is similar to a phenomenon observed before, where radiolabelled Tim18, Tim22, Tim54, and Tim23 showed an improved incorporation into the TIM22 and TIM23 complexes when the corresponding endogenous protein was downregulated or absent [19, 28]. To address whether Mpc1 import and assembly depend on the carrier pathway, the *MPC1* gene was deleted in WT, *tim22-14*, and *tim10-2* mutants. When [$^{35}$S]-labeled Mpc1 was imported in *tim22-14* and *tim10-2* mitochondria, Mpc1 assembly was affected (Figure 3C), whereas import and assembly of the presequence pathway substrate Atp5 were not compromised (Figure 3D). Moreover, the mutant cells did not display a significant difference in inner membrane potential in comparison to the WT (Figure 3E).

---

(F) Proteomic analyses of *tim22-14* versus WT mitochondria. Mean log$_2$ ratio-intensity plot mitochondria are shown. The ratio-intensity mean plot shows the effect of loss of Tim22 function on the abundance of mitochondrial carrier proteins (in red, blue for MPC subunits). Filled circles indicate proteins significantly altered in abundance.

(G) Immunodetection of selected proteins in WT and *tim22-14* mitochondria. Δψ, membrane potential; N, N terminus; C, C terminus; Cyt., cytoplasm; OMM, outer mitochondrial membrane; IMM, inner mitochondrial membrane; IMS, intermembrane space; Matr., matrix.

See also Figure S1 and Table S1.
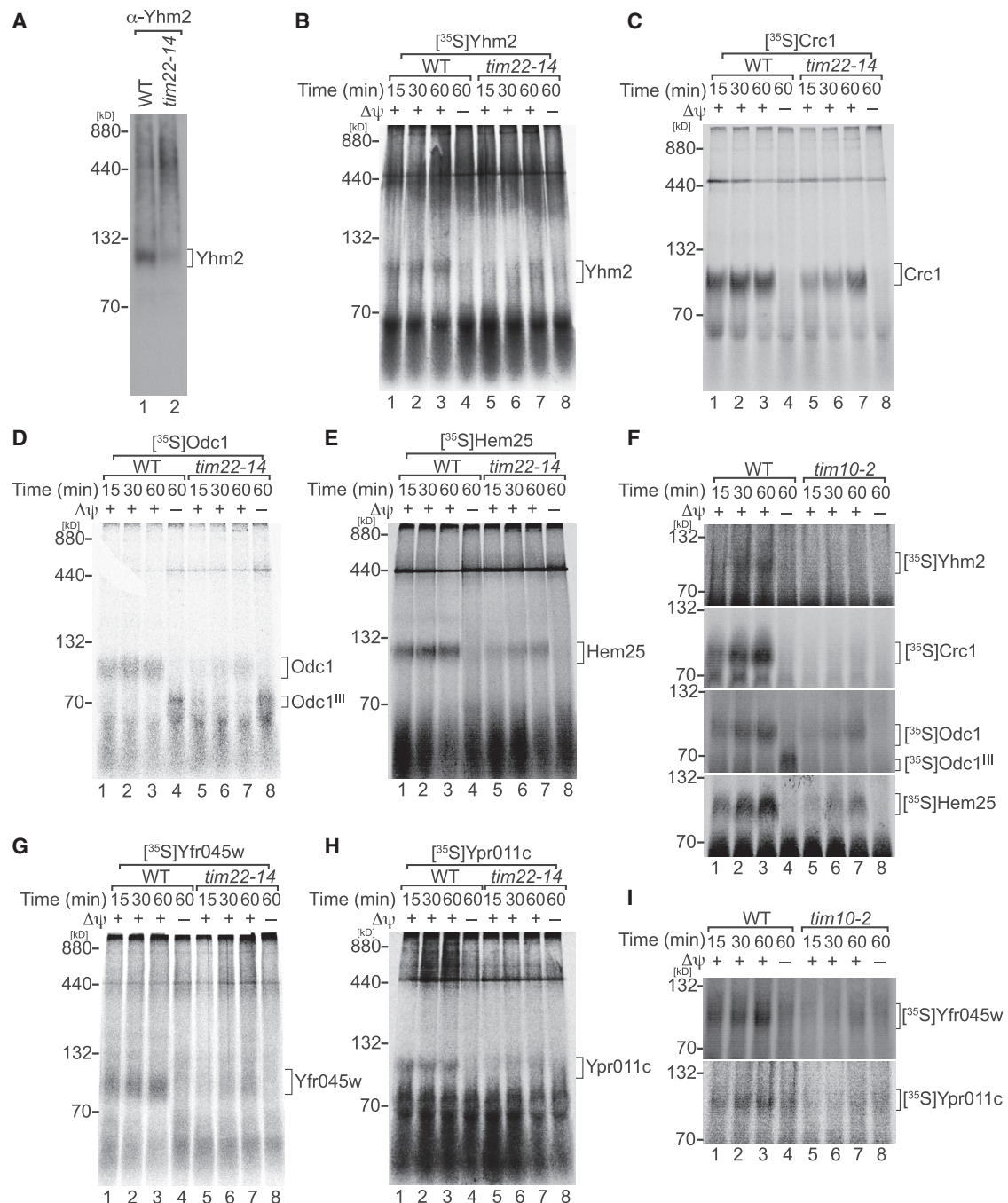
**Figure 2. Mitochondrial Carrier Biogenesis Is Affected in *tim22-14* and *tim10-2* Mutants**

(A) BN-PAGE analysis of Yhm2 in mitochondria isolated from cells grown for 15 h at the non-permissive temperature (37°C).

(B–F) [$^{35}$S]-labeled (B) Yhm2, (C) Crc1, (D) Odc1, and (E) Hem25 were imported into WT and *tim22-14* mitochondria and (F) into WT and *tim10-2* mitochondria.

(G and H) [$^{35}$S]-labeled (G) Yfr045w and (H) Ypr011c were imported into WT and *tim22-14* mitochondria.

(I) Both proteins were imported into WT and *tim10-2* mitochondria. In all import experiments, analyses were carried out by BN-PAGE and digital autoradiography. See also Figure S2.

Mpc3 and Mpc2 imports were also affected in *tim22-14* (73.4% and 51.1% of WT, respectively) and *tim10-2* (59.7% and 51.8%, respectively) mitochondria (Figures 3F, 3H, and S3B). Furthermore, Mpc3 and Mpc2 import was reduced in *tom70/71ΔΔ* receptor mutant mitochondria, supporting the

idea that these proteins are imported along the carrier pathway (Figure S3C). To exclude that the reduction of Mpc3 assembly in *tim22-14* was due to inactivation of Tim22 and not indirectly caused by reduced levels of Mpc1 in this strain, we imported Mpc3 into *mpc1Δ* and *tim22-14/mpc1Δ* mitochondria. Indeed,
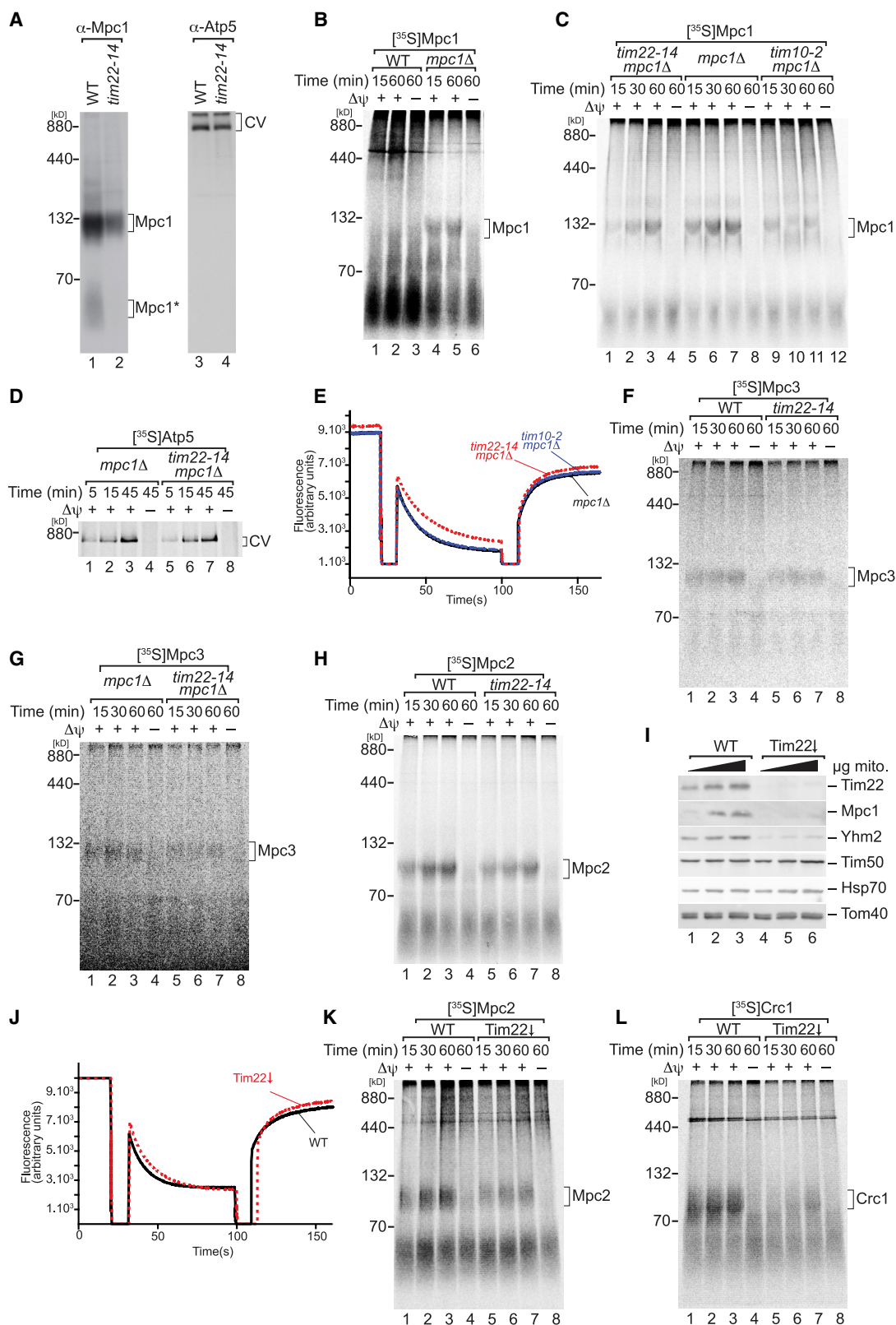
**Figure 3. MPC Subunits Are Imported along the Carrier Pathway**

(A) Isolated mitochondria from WT and *tim22-14* cells grown for 15 h at the non-permissive temperature (37°C) were solubilized and analyzed by BN-PAGE and immunoblotting.
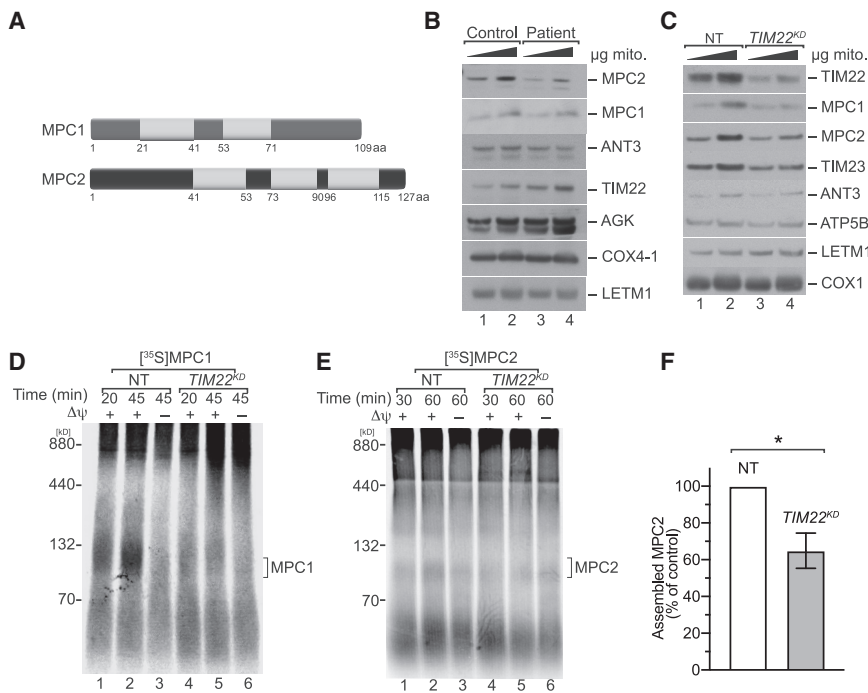
**Figure 4. MPC Assembly Is Affected upon Defects in TIM22 in Human Mitochondria**

(A) Topology of human MPC1 and MPC2.

(B) Isolated mitochondria from control and patient fibroblast were analyzed by SDS-PAGE and western blotting.

(C) HEK293T cells were treated with TIM22-specific small interfering RNA (siRNA) or non-targeting siRNA (NT). Isolated mitochondria were subjected to SDS-PAGE and western blotting.

(D and E) [35S]-labeled (D) MPC1 and (E) MPC2 were imported into isolated mitochondria from HEK293T cells transfected either with non-targeting (NT) or TIM22-specific siRNA ($TIM22^{KD}$).

(F) Quantification of assembled MPC2 at 60 min (mean ± SEM, n = 3) (*p < 0.05, unpaired t test, two tails). aa, amino acid; $\Delta\psi$, membrane potential.

## Pyruvate Carrier Biogenesis Is Affected in TIM22 Patient Mitochondria

Human MPC1 and MPC2 are similar to their yeast counterparts in that they contain two and three putative TM segments, respectively (Figure 4A). The composition of the human carrier translocase differs from the yeast counterpart [32]. Recently, a mutation in the conserved channel-forming TIM22 subunit has been associated with a human disorder [33]. Therefore, we analyzed MPC1 and MPC2 steady-state levels in isolated mitochondria from control and TIM22 patient fibroblasts. The amount of MPC1 was slightly reduced, whereas MPC2 levels were found to be significantly decreased in patient mitochondria (Figure 4B). When we assessed MPC proteins under conditions of TIM22 knockdown in HEK293T cells, we similarly observed reduced amounts of MPC1 and MPC2 in comparison with the control (Figure 4C). Therefore, we assessed in vitro import and assembly of MPC1 and MPC2 into isolated HEK293T mitochondria after TIM22 knockdown. Assembly of both proteins into the MPC complex was significantly reduced when TIM22 function was compromised (Figures 4D–4F). Accordingly, the import of MPC1 and MPC2 depends on the TIM22 complex in human mitochondria. Despite the fact that the composition of the TIM22 complex is different in yeast and human mitochondria, recognition of non-canonical substrates appears to be a conserved mechanism.

a reduction in assembly was observed in *tim22-14/mpc1Δ* mutant mitochondria (72.79% of WT), indicating dependence of Mpc3 import on Tim22 (Figure 3G). To corroborate that the MPC subunit biogenesis was dependent on Tim22, a second approach was established in which Tim22 levels were reduced with the aid of the GAL1 promoter. Steady-state levels of Tim22 and Mpc1 in mitochondria were drastically reduced, and also the levels of Yhm2 dropped drastically upon Tim22 depletion (Figure 3I). Because the mitochondrial membrane potential was not affected in Tim22-depleted mitochondria (Figure 3J), we imported radiolabelled Mpc2 and Crc1 in vitro into mutant and WT mitochondria. Both Mpc2 (54.9% of WT) and Crc1 assembly were reduced upon depletion of Tim22. Accordingly, *tim22-14* mutant cells and Tim22-downregulated cells displayed similar effects on carrier protein import (Figure 3K and 3L). Finally, to confirm that the MPC subunit import was dependent only on the carrier pathway, the Mpc3 import was carried out in Tim23$^{N150A}$ mutant mitochondria. In this mutant, Mpc3 import and assembly were not compromised. Instead, we observed a slight increase in the Mpc3 assembly (Figure S3D). This effect was similar to what was shown for the AAC assembly in the same strain or other presequence translocase mutants [29–31].

(B and C) [35S]-labeled Mpc1 was imported into (B) WT and *mpc1Δ* mitochondria and (C) *mpc1Δ*, *tim22-14/mpc1Δ*, and *tim10-2/mpc1Δ* mitochondria.

(D) [35S]-labeled Atp5 was imported into *mpc1Δ* and *tim22-14/mpc1Δ* mitochondria.

(E) Membrane potential measurement of *mpc1Δ*, *tim22-14/mpc1Δ*, and *tim10-2/mpc1Δ* mitochondria.

(F and G) [35S]-labeled Mpc3 was imported into (F) WT and *tim22-14* mitochondria and (G) *mpc1Δ* and *tim22-14/mpc1Δ* mitochondria.

(H) [35S]-labeled Mpc2 was imported into WT and *tim22-14* mitochondria.

(I) Purified mitochondria from WT and Tim22-downregulated (Tim22↓) cells were analyzed by SDS-PAGE and western blotting.

(J) Membrane potential measurement of WT and Tim22-downregulated mitochondria.

(K and L) [35S]-labeled (K) Mpc2 and (L) Crc1 were imported into WT and Tim22-downregulated mitochondria. In all import experiments, analyses were carried out by BN-PAGE and digital autoradiography. $\Delta\psi$, membrane potential.

See also Figure S3.

## DISCUSSION

In this study, we performed proteomic analyses of *tim22-14* yeast mitochondria to define substrates of the carrier transport pathway. Our quantitative analyses identified functionally defined (Yhm2, Crc1, Odc1, and Hem25) and undefined proteins (Yfr045w and Ypr011c) as substrates of the carrier pathway. Transport of the tested proteins was affected to varying degrees in different pathway mutants in *in vitro* import analyses. It is conceivable that differences in the biophysical properties of the transmembrane spans of the individual protein or differences in their internal targeting signals are at the heart of these distinct requirements and that conditional mutants display a certain substrate specificity. Moreover, our analyses identified pyruvate carrier subunits as non-canonical substrates of the carrier pathway. Reduced levels of MPC1 and MPC2 were also apparent in a patient compromised in carrier import and upon depletion of TIM22 in human cells. Therefore, these proteins are substrates of the carrier pathway in yeast and in human mitochondria despite the drastic differences in the organization of the translocase. These precursors with two or three transmembrane segments do not fit with current concepts of a membrane insertion mechanism of polypeptides in hairpin loops mediated by TIM22 [34, 35]. A net positive charge of the matrix-facing loops has been considered as one of the driving factors for carrier proteins across the membrane [34]. Sequence analysis of the MPC proteins revealed that the matrix-facing N termini are positively charged. It is tempting to speculate that these drive the translocation across the inner membrane by the TIM22 complex. Detailed biochemical analyses will be required to understand the translocation process in the light of these unexpected findings.

## STAR★METHODS

Detailed methods are provided in the online version of this paper and include the following:

- KEY RESOURCES TABLE
- LEAD CONTACT AND MATERIALS AVAILABILITY
- EXPERIMENTAL MODEL AND SUBJECT DETAILS
  - Yeast growth and handling
  - Cell culture and knockdown experiments
- METHOD DETAILS
  - Isolation of mitochondria
  - Microscopy of yeast cells
  - Import of precursor proteins
  - Membrane potential measurement
  - Reduction and alkylation of proteins and tryptic digestion
  - Dimethyl labeling of peptides on StageTips
  - Desalting and fractionation of samples
  - LC-MS analysis
  - MS data analysis
- QUANTIFICATION AND STATISTICAL ANALYSIS
- DATA AND CODE AVAILABILITY

## SUPPLEMENTAL INFORMATION

Supplemental Information can be found online at https://doi.org/10.1016/j.cub.2020.01.024.

## AUTHOR CONTRIBUTIONS

Conceptualization, P.R.; Methodology, P.R., B.W., R.G., and I.S.; Investigation, R.G., L.D.C.-Z., I.S., D.P.-G., and S.C.; Resources, P.R., B.W., J.M., and B.G.; Writing – Original Draft, P.R., R.G., L.D.C.-Z., D.P.-G., I.S., and B.W.; Writing – Review & Editing, P.R., R.G., L.D.C.-Z., D.P.-G., and B.W.; Funding Acquisition, P.R., B.W., and J.M.; Supervision, P.R. and B.W.

## DECLARATION OF INTERESTS

The authors declare no competing interests.

## REFERENCES

1. Brandner, K., Rehling, P., and Truscott, K.N. (2005). The carboxyl-terminal third of the dicarboxylate carrier is crucial for productive association with the inner membrane twin-pore translocase. J. Biol. Chem. *280*, 6215–6221.

2. Brix, J., Ziegler, G.A., Dietmeier, K., Schneider-Mergener, J., Schulz, G.E., and Pfanner, N. (2000). The mitochondrial import receptor Tom70: identification of a 25 kDa core domain with a specific binding site for preproteins. J. Mol. Biol. *303*, 479–488.

3. Pfanner, N., Hoeben, P., Tropschug, M., and Neupert, W. (1987). The carboxyl-terminal two-thirds of the ADP/ATP carrier polypeptide contains sufficient information to direct translocation into mitochondria. J. Biol. Chem. *262*, 14851–14854.

4. Hines, V., Brandt, A., Griffiths, G., Horstmann, H., Brütsch, H., and Schatz, G. (1990). Protein import into yeast mitochondria is accelerated by the outer membrane protein MAS70. EMBO J. *9*, 3191–3200.

5. Söllner, T., Pfaller, R., Griffiths, G., Pfanner, N., and Neupert, W. (1990). A mitochondrial import receptor for the ADP/ATP carrier. Cell *62*, 107–115.

6. Young, J.C., Hoogenraad, N.J., and Hartl, F.U. (2003). Molecular chaperones Hsp90 and Hsp70 deliver preproteins to the mitochondrial import receptor Tom70. Cell *112*, 41–50.

7. Adam, A., Endres, M., Sirrenberg, C., Lottspeich, F., Neupert, W., and Brunner, M. (1999). Tim9, a new component of the TIM22.54 translocase in mitochondria. EMBO J. *18*, 313–319.

8. Koehler, C.M., Merchant, S., Oppliger, W., Schmid, K., Jarosch, E., Dolfini, L., Junne, T., Schatz, G., and Tokatlidis, K. (1998). Tim9p, an essential partner subunit of Tim10p for the import of mitochondrial carrier proteins. EMBO J. *17*, 6477–6486.

9. Sirrenberg, C., Endres, M., Fölsch, H., Stuart, R.A., Neupert, W., and Brunner, M. (1998). Carrier protein import into mitochondria mediated by

the intermembrane proteins Tim10/Mrs11 and Tim12/Mrs5. Nature *391*, 912–915.

10. Truscott, K.N., Wiedemann, N., Rehling, P., Müller, H., Meisinger, C., Pfanner, N., and Guiard, B. (2002). Mitochondrial import of the ADP/ATP carrier: the essential TIM complex of the intermembrane space is required for precursor release from the TOM complex. Mol. Cell. Biol. *22*, 7780–7789.

11. Webb, C.T., Gorman, M.A., Lazarou, M., Ryan, M.T., and Gulbis, J.M. (2006). Crystal structure of the mitochondrial chaperone TIM9.10 reveals a six-bladed alpha-propeller. Mol. Cell *21*, 123–133.

12. Weinhäupl, K., Lindau, C., Hessel, A., Wang, Y., Schütze, C., Jores, T., Melchionda, L., Schönfisch, B., Kalbacher, H., Bersch, B., et al. (2018). Structural Basis of Membrane Protein Chaperoning through the Mitochondrial Intermembrane Space. Cell *175*, 1365–1379.

13. Kovermann, P., Truscott, K.N., Guiard, B., Rehling, P., Sepuri, N.B., Müller, H., Jensen, R.E., Wagner, R., and Pfanner, N. (2002). Tim22, the essential core of the mitochondrial protein insertion complex, forms a voltage-acti- vated and signal-gated channel. Mol. Cell *9*, 363–373.

14. Rehling, P., Model, K., Brandner, K., Kovermann, P., Sickmann, A., Meyer, H.E., Kühlbrandt, W., Wagner, R., Truscott, K.N., and Pfanner, N. (2003). Protein insertion into the mitochondrial inner membrane by a twin-pore translocase. Science *299*, 1747–1751.

15. Sirrenberg, C., Bauer, M.F., Guiard, B., Neupert, W., and Brunner, M. (1996). Import of carrier proteins into the mitochondrial inner membrane mediated by Tim22. Nature *384*, 582–585.

16. Káldi, K., Bauer, M.F., Sirrenberg, C., Neupert, W., and Brunner, M. (1998). Biogenesis of Tim23 and Tim17, integral components of the TIM machin- ery for matrix-targeted preproteins. EMBO J. *17*, 1569–1576.

17. Leuenberger, D., Bally, N.A., Schatz, G., and Koehler, C.M. (1999). Different import pathways through the mitochondrial intermembrane space for inner membrane proteins. EMBO J. *18*, 4816–4822.

18. Peikert, C.D., Mani, J., Morgenstern, M., Käser, S., Knapp, B., Wenger, C., Harsman, A., Oeljeklaus, S., Schneider, A., and Warscheid, B. (2017). Charting organellar importomes by quantitative mass spectrometry. Nat. Commun. *8*, 15272.

19. Wagner, K., Gebert, N., Guiard, B., Brandner, K., Truscott, K.N., Wiedemann, N., Pfanner, N., and Rehling, P. (2008). The assembly pathway of the mitochondrial carrier translocase involves four preprotein translocases. Mol. Cell. Biol. *28*, 4251–4260.

20. Melin, J., Kilisch, M., Neumann, P., Lytovchenko, O., Gomkale, R., Schendzielorz, A., Schmidt, B., Liepold, T., Ficner, R., Jahn, O., et al. (2015). A presequence-binding groove in Tom70 supports import of Mdl1 into mitochondria. Biochim. Biophys. Acta *1853*, 1850–1859.

21. Belenkiy, R., Haefele, A., Eisen, M.B., and Wohlrab, H. (2000). The yeast mitochondrial transport proteins: new sequences and consensus resi- dues, lack of direct relation between consensus residues and transmem- brane helices, expression patterns of the transport protein genes, and pro- tein-protein interactions with other proteins. Biochim. Biophys. Acta *1467*, 207–218.

22. Todisco, S., Di Noia, M.A., Castegna, A., Lasorsa, F.M., Paradies, E., and Palmieri, F. (2014). The Saccharomyces cerevisiae gene YPR011c en- codes a mitochondrial transporter of adenosine 5′-phosphosulfate and 3′-phospho-adenosine 5′-phosphosulfate. Biochim. Biophys. Acta *1837*, 326–334.

23. Bricker, D.K., Taylor, E.B., Schell, J.C., Orsak, T., Boutron, A., Chen, Y.-C., Cox, J.E., Cardon, C.M., Van Vranken, J.G., Dephoure, N., et al. (2012). A mitochondrial pyruvate carrier required for pyruvate uptake in yeast, Drosophila, and humans. Science *337*, 96–100.

24. Herzig, S., Raemy, E., Montessuit, S., Veuthey, J.-L., Zamboni, N., Westermann, B., Kunji, E.R.S., and Martinou, J.-C. (2012). Identification and functional expression of the mitochondrial pyruvate carrier. Science *337*, 93–96.

25. Palmieri, F. (2004). The mitochondrial transporter family (SLC25): physio- logical and pathological implications. Pflugers Arch. *447*, 689–709.

26. Tavoulari, S., Thangaratnarajah, C., Mavridou, V., Harbour, M.E., Martinou, J.-C., and Kunji, E.R.S. (2019). The yeast mitochondrial pyruvate carrier is a hetero-dimer in its functional state. EMBO J. *38*. Published on- line May 15, 2019. https://doi.org/10.15252/embj.2018100785.

27. Bender, T., Pena, G., and Martinou, J.-C. (2015). Regulation of mitochon- drial pyruvate uptake by alternative pyruvate carrier complexes. EMBO J. *34*, 911–924.

28. van der Laan, M., Meinecke, M., Dudek, J., Hutu, D.P., Lind, M., Perschil, I., Guiard, B., Wagner, R., Pfanner, N., and Rehling, P. (2007). Motor-free mitochondrial presequence translocase drives membrane integration of preproteins. Nat. Cell Biol. *9*, 1152–1159.

29. Geissler, A., Chacinska, A., Truscott, K.N., Wiedemann, N., Brandner, K., Sickmann, A., Meyer, H.E., Meisinger, C., Pfanner, N., and Rehling, P. (2002). The mitochondrial presequence translocase: an essential role of Tim50 in directing preproteins to the import channel. Cell *111*, 507–518.

30. Frazier, A.E., Dudek, J., Guiard, B., Voos, W., Li, Y., Lind, M., Meisinger, C., Geissler, A., Sickmann, A., Meyer, H.E., et al. (2004). Pam16 has an essen- tial role in the mitochondrial protein import motor. Nat. Struct. Mol. Biol. *11*, 226–233.

31. Denkert, N., Schendzielorz, A.B., Barbot, M., Versemann, L., Richter, F., Rehling, P., and Meinecke, M. (2017). Cation selectivity of the prese- quence translocase channel Tim23 is crucial for efficient protein import. eLife *6*. Published online August 31, 2017. https://doi.org/10.7554/eLife. 28324.

32. Kang, Y., Fielden, L.F., and Stojanovski, D. (2018). Mitochondrial protein transport in health and disease. Semin. Cell Dev. Biol. *76*, 142–153.

33. Pacheu-Grau, D., Callegari, S., Emperador, S., Thompson, K., Aich, A., Topol, S.E., Spencer, E.G., McFarland, R., Ruiz-Pesini, E., Torkamani, A., et al. (2018). Mutations of the mitochondrial carrier translocase channel subunit TIM22 cause early-onset mitochondrial myopathy. Hum. Mol. Genet. *27*, 4135–4144.

34. Rehling, P., Brandner, K., and Pfanner, N. (2004). Mitochondrial import and the twin-pore translocase. Nat. Rev. Mol. Cell Biol. *5*, 519–530.

35. Chacinska, A., Koehler, C.M., Milenkovic, D., Lithgow, T., and Pfanner, N. (2009). Importing mitochondrial proteins: machineries and mechanisms. Cell *138*, 628–644.

36. Sikorski, R.S., and Hieter, P. (1989). A system of shuttle vectors and yeast host strains designed for efficient manipulation of DNA in Saccharomyces cerevisiae. Genetics *122*, 19–27.

37. Callegari, S., Richter, F., Chojnacka, K., Jans, D.C., Lorenzi, I., Pacheu- Grau, D., Jakobs, S., Lenz, C., Urlaub, H., Dudek, J., et al. (2016). TIM29 is a subunit of the human carrier translocase required for protein transport. FEBS Lett. *590*, 4147–4158.

38. Wach, A., Brachat, A., Pöhlmann, R., and Philippsen, P. (1994). New het- erologous modules for classical or PCR-based gene disruptions in Saccharomyces cerevisiae. Yeast *10*, 1793–1808.

39. Meisinger, C., Pfanner, N., and Truscott, K.N. (2006). Isolation of yeast mitochondria. Methods Mol. Biol. *313*, 33–39.

40. Lazarou, M., Smith, S.M., Thorburn, D.R., Ryan, M.T., and McKenzie, M. (2009). Assembly of nuclear DNA-encoded subunits into mitochondrial complex IV, and their preferential integration into supercomplex forms in patient mitochondria. FEBS J. *276*, 6701–6713.

41. Mohanraj, K., Wasilewski, M., Benincá, C., Cysewski, D., Poznanski, J., Sakowska, P., Bugajska, Z., Deckers, M., Dennerlein, S., Fernandez- Vizarra, E., et al. (2019). Inhibition of proteasome rescues a pathogenic variant of respiratory chain assembly factor COA7. EMBO Mol. Med. *11*. Published online March 18, 2019. https://doi.org/10.15252/emmm. 201809561.

42. Aich, A., Wang, C., Chowdhury, A., Ronsör, C., Pacheu-Grau, D., Richter- Dennerlein, R., Dennerlein, S., and Rehling, P. (2018). COX16 promotes COX2 metallation and assembly during respiratory complex IV biogenesis. eLife *7*. Published online January 30, 2018. https://doi.org/10.7554/eLife. 32572.

43. Topf, U., Suppanz, I., Samluk, L., Wrobel, L., Böser, A., Sakowska, P., Knapp, B., Pietrzyk, M.K., Chacinska, A., and Warscheid, B. (2018). Quantitative proteomics identifies redox switches for global translation modulation by mitochondrially produced reactive oxygen species. Nat. Commun. *9*, 324.

44. Rappsilber, J., Mann, M., and Ishihama, Y. (2007). Protocol for micro-purification, enrichment, pre-fractionation and storage of peptides for proteomics using StageTips. Nat. Protoc. *2*, 1896–1906.

45. Cox, J., and Mann, M. (2008). MaxQuant enables high peptide identification rates, individualized p.p.b.-range mass accuracies and proteome-wide protein quantification. Nat. Biotechnol. *26*, 1367–1372.

46. Cox, J., Neuhauser, N., Michalski, A., Scheltema, R.A., Olsen, J.V., and Mann, M. (2011). Andromeda: a peptide search engine integrated into the MaxQuant environment. J. Proteome Res. *10*, 1794–1805.

47. Cox, J., and Mann, M. (2012). 1D and 2D annotation enrichment: a statistical method integrating quantitative proteomics with complementary high-throughput data. BMC Bioinformatics *13* (*Suppl 16*), S12.

48. Morgenstern, M., Stiller, S.B., Lübbert, P., Peikert, C.D., Dannenmaier, S., Drepper, F., Weill, U., Höß, P., Feuerstein, R., Gebert, M., et al. (2017). Definition of a High-Confidence Mitochondrial Proteome at Quantitative Scale. Cell Rep. *19*, 2836–2852.

# STAR★METHODS

## KEY RESOURCES TABLE

| REAGENT or RESOURCE | SOURCE | IDENTIFIER |
| --- | --- | --- |
| Antibodies | | |
| Rabbit polyclonal anti-Tim22 | This paper | #164 |
| Rabbit polyclonal anti-Tim54 | This paper | #215 |
| Rabbit polyclonal anti-Tim18 | This paper | #233 |
| Rabbit polyclonal anti-Tim23 | This paper | #3846 |
| Rabbit polyclonal anti-Tim17 | This paper | #4968 |
| Rabbit polyclonal anti-Tim50 | This paper | #3314 |
| Rabbit polyclonal anti-Tim21 | This paper | #3111 |
| Rabbit polyclonal anti-Tim44 | This paper | #3869 |
| Rabbit polyclonal anti-Tom40 | This paper | #4901 |
| Rabbit polyclonal anti-Hsp70 | This paper | #4945 |
| Rabbit polyclonal anti-Mir1 | This paper | #171 |
| Rabbit polyclonal anti-Aac2 | This paper | #51 |
| Rabbit polyclonal anti-Yhm2 | This paper | #3053 (Freiburg) |
| Rabbit polyclonal anti-Mpc1 | This paper | #5021 (Freiburg) |
| Rabbit polyclonal anti-Atp20 | This paper | #1517 |
| Rabbit polyclonal anti-Mic10 | This paper | #345 |
| Rabbit polyclonal anti-Atp5 | This paper | #1546 |
| Rabbit polyclonal anti-MPC1 | Thermo Fisher Scientific | Cat# PA5-60929; RRID: AB_2638597 |
| Rabbit polyclonal anti-MPC2 | Proteintech | Cat# 20049-1-AP |
| Rabbit polyclonal anti-TIM22 | Proteintech | Cat# 14927-1-AP; RRID: AB_11183050 |
| Rabbit polyclonal anti-AGK | This paper | #5045 |
| Rabbit polyclonal anti-ANT3 | Proteintech | Cat# 14841-1-AP; RRID: AB_2190371 |
| Rabbit polyclonal anti-TIM23 | This paper | #1526 |
| Rabbit polyclonal anti-LETM1 | This paper | #0538 |
| Rabbit polyclonal anti-COX1 | This paper | #5120 |
| Rabbit polyclonal anti-COX4-1 | This paper | #1522 |
| Rabbit polyclonal anti-ATP5B | This paper | #4826 |
| Goat anti Rabbit IgG (H+L) HRPO | Jackson ImmunoResearch Labs | Cat# 111-035-144; RRID: AB_2307391 |
| Chemicals, Peptides, and Recombinant Proteins | | |
| Digitonin | Merck Millipore | Cat# 300410 |
| MitoTrackerTM Orange CMTMRos | Thermo Fisher Scientific | Cat# M-7510 |
| 3,3′-Dipropylthiadicarbocyanine Iodide (DiSC$_3$) | Invitrogen | Cat# D306 |
| deuterated cyanoborohyride NaBD$_3$CN | Sigma-Aldrich | Cat# 190020 |
| deuterated formaldehyde CD$_2$O | Sigma-Aldrich | Cat# 492620 |
| deuterated $^{13}$C-labeled formaldehyde $^{13}$CD$_2$O | Sigma-Aldrich | Cat# 596388 |
| [$^{35}$S] methionine | Hartmann Analytic | Cat# SCM-01 |
| Critical Commercial Assays | | |
| KOD Hot Start DNA Polymerase | Merck | Cat# 71086-3 |
| mMessagemMachine SP6 transcription kit | Invitrogen | Cat# AM1340 |
| Flexi Rabbit Reticulocyte Lysate System | Promega | Cat# L4540 |
| Experimental Models: Cell Lines | | |
| HEK293-Flp-InTM T-RexTM (HEK293T) Cell Line | ThermoFisher Scientific | RRID: CVCL_U421 |
| Control Fibroblasts (immortalized) | [33] | N/A |
| TIM22 Patient Fibroblasts (immortalized) | [33] | N/A |

*Continued*

| REAGENT or RESOURCE | SOURCE | IDENTIFIER |
|---|---|---|
| **Experimental Models: Organisms/Strains** | | |
| YPH499 MATa *ade2-101, his3-Δ200, leu2-Δ1, ura3-52, trp1-Δ63, lys2-801* | [36] | Yeast collection# 13 |
| BY4741 MATa *his3Δ1, leu2Δ0, met15Δ0, ura3Δ0* | EUROSCARF | http://euroscarf.de/index.php?name=News |
| BY4741 *yfr045wΔ::KanMX4* | EUROSCARF | http://euroscarf.de/index.php?name=News |
| BY4741 *ypr011cΔ::KanMX4* | EUROSCARF | http://euroscarf.de/index.php?name=News |
| BY4741 *mpc1Δ::KanMX4* | EUROSCARF | http://euroscarf.de/index.php?name=News |
| *tim22-14:* YPH499 *tim22-M4* | [19] | Yeast collection# 172 |
| *tim10-2:* YPH499 *tim10::ADE2* | [10] | Yeast collection# 173 |
| YPH499 *mpc1Δ:* YPH499 *mpc1Δ::KanMX4* | This paper | N/A |
| *tim22-14/mpc1Δ:* YPH499 *tim22-M4 mpc1Δ::KanMX4* | This paper | N/A |
| *tim10-2/mpc1Δ:* YPH499 *tim10::ADE2 mpc1Δ::KanMX4* | This paper | N/A |
| *tom70/71 ΔΔ:* YPH499 *tom70Δ::HIS3, tom71Δ::KanMX4* | [20] | Yeast collection# 796 |
| Tim22↓: YPH499 *KanMX-pGal1-Tim22* | This paper | N/A |
| **Oligonucleotides** | | |
| TIM22 siRNA GUG-AGG-AGC-AGA-AGA-UGA | [37] | N/A |
| **Recombinant DNA** | | |
| Plasmid: GFP-Mir1 | This paper | pRG3 |
| pFA6a-KanMX6 | [38] | Plasmid# R66 |
| **Software and Algorithms** | | |
| ImageQuantTL v8.1 | GE Healthcare | https://www.gelifesciences.com/en/us/shop/protein-analysis/molecular-imaging-for-proteins/imaging-software/imagequant-tl-8-1-p-00110 |
| ImageJ v1.47 | NIH | https://imagej.nih.gov/ij/download.html |
| Geneious v9.1.2 | Biomatters Ltd | https://www.geneious.com/download/ |
| Prism 8 | GraphPad Software | https://www.graphpad.com/scientific-software/prism/ |

## LEAD CONTACT AND MATERIALS AVAILABILITY

Further information and requests for resources and reagents should be directed to and will be fulfilled by the Lead Contact, Peter Rehling (peter.rehling@medizin.uni-goettingen.de). This study did not generate new unique reagents.

## EXPERIMENTAL MODEL AND SUBJECT DETAILS

### Yeast growth and handling

*S. cerevisiae* strains used in this study were YPH499 and BY4741. The genotypes are listed in the Key Resources Table. Cells were grown in YP media (1% yeast extract, 2% peptone) containing 2% glucose (YPD) or 3% glycerol (YPG) as a carbon source. YPH499, BY4741, *yfr045wΔ, ypr011cΔ* and *tom70/tom71 ΔΔ* [20] strains were grown at 30°C with shaking. Temperature sensitive (ts) strains *tim22-14* [19] and *tim10-2* [10] were cultivated at 24°C and 19°C, respectively. For proteomic analysis, incubation of temperature conditional mutant strains was carried out at 37°C for indicated times. For growth on plates, 1.5% agar was added to synthetic YPD, YPG or YPL (3% lactate, pH 5.0) media. For comparing growth of different strains, serial dilutions of an overnight growing culture were prepared and plated on appropriate plates. These plates were incubated at 24°C, 30°C, and 37°C for 3-5 days. GFP-Mir1 was expressed in YPH499 and *tim22-14* cells. For this *MIR1* was cloned into pUG36. The resulting plasmid (pRG3) was transformed into yeast strains. Transformants were selected on SD-Ura (selective media lacking uracil). Deletion of the *MPC1* open reading frame in YPH499, *tim10-2,* and *tim22-14* was achieved by homologous recombination following transformation of a PCR product containing the KanMX gene flanked by regions complementary to the MPC1 UTRs and subsequent selection of Kan-resistant transformants. For Tim22↓ strain, the Gal1 promoter with a Kanamycin marker was integrated 5′ upstream of the open reading frame of Tim22. The

Gal1 promoter is activated in the presence of Galactose and repressed in Glucose. For downregulation of Tim22 expression, yeast cells were pre-cultured in YP media with 3% Lactate, 1% Galactose and 1% Raffinose pH 5.0 for 25 hours at 30°C. Subsequently, the cells were cultured in YP media with 3% Lactate and 0.1% Glucose pH 5.0 for 10 hours at 30°C.

### Cell culture and knockdown experiments

Immortalized fibroblasts and HEK293T cells were cultured in DMEM, supplemented with 10% (v/v) heat-inactivated fetal bovine serum (Biochrom, Berlin, Germany), 2 mM L-glutamine, 1 mM sodium pyruvate and 50 μg/ml uridine, and incubated at 37°C with 5% $CO_2$. Mitochondria from control and patient fibroblast were isolated after incubating the cells at 50°C for 5 hours and were subjected to SDS-PAGE and western blotting.

TIM22 knock down was performed as previously described [37]. An siRNA targeting TIM22 (GUG-AGG-AGC-AGA-AGA-UGA) and the corresponding non-targeting control were purchased from Eurogentec (Liege, Belgium). A concentration of approximately $1.5x10^6$ cells/25 $cm^2$ flask were transfected with 16 nM siRNA. Lipofectamine RNAiMAX (Invitrogen, CA, USA) in OptiMEM-I medium (GIBCO, Thermo Fisher Scientific, MA, USA) was used for transfection, following the manufacturer's instructions. Cells were transfected for 72 h and used for subsequent analyses.

## METHOD DETAILS

### Isolation of mitochondria

Differential centrifugation of yeast extracts was carried out to isolate mitochondria [39]. Unless otherwise stated, wild-type, *tim22-14* and *tim10-2* yeast cells were cultured in YPG at 30°C, 24°C, or 19°C to $OD_{600}$ of 1.5-2.5 and harvested. The pellet was washed with water and then treated in DTT buffer (10 mM DTT, 100 mM Tris/$H_2SO_4$, pH 9.4) for 30 min at appropriate temperature with shaking. Subsequently, cells were washed and treated with Zymolyase buffer (20 mM $KPO_4$, pH 7.4, 1.2 M sorbitol, and 0.57 mg/L zymolyase) for 1 h with shaking at the appropriate temperature. Cells were harvested and washed with zymolyase buffer. Cold homogenization buffer (600 mM sorbitol, 10 mM Tris/HCl, pH 7.4, 1 g/L BSA, 1 mM PMSF, and 1 mM EDTA) was added to the pellet and cells were homogenized using a homogenizer. Mitochondria were obtained by differential centrifugation and resuspended in SEM buffer (250 mM sucrose, 20 mM MOPS/KOH pH 7.2, 1 mM EDTA). They were aliquoted in appropriate volume, flash frozen in liquid nitrogen, and stored at −80°C. Steady-state analysis of proteins was carried out using SDS-PAGE followed by immunodecoration.

For experiments involving human cells, mitochondria used for western blotting purposes were isolated by differential centrifugation as previously described [40]. Briefly, PBS recovered cells were dissolved in isolation buffer (300 mM trehalose, 10 mM KCl, 10 mM HEPES pH 7.4, 2mg/ml BSA, and 2mM PMSF). Cells were subsequently homogenized on ice using a Potter S homogenizer. Cell debris was removed by a first centrifugation step at 400 *x g* for 10 min at 4°C and after recovering the supernatant a second one at 800 *x g* for 7 min at 4°C. Mitochondria were collected by centrifugation at 10,000 *x g* for 10 min at 4°C. Freshly isolated mitochondria were washed in isolation buffer lacking BSA once and protein concentrations were determined by Bradford assay. For import experiments, mitochondria were isolated as previously described [41]. Briefly, cells were resuspended in ice-cold isotonic buffer (10 mM MOPS pH 7.2, 225 mM sucrose, 75 mM mannitol, and 1 mM EGTA) supplemented with 2 mM PMSF and 2 mg/ml BSA and subjected to centrifugation at 1,000 *x g* for 5 min at 4°C. The cell pellet was subsequently resuspended in cold hypotonic buffer (10 mM MOPS pH 7.2, 100 mM sucrose, and 1 mM EGTA) and incubated on ice for 7 min. The cell suspension was homogenized in a Dounce glass homogenizer. Cold hypertonic buffer (1.25 M sucrose and 10 mM MOPS pH 7.2) was used to restore isotonic condition and added to the cell homogenate. The homogenate was subjected to centrifugation at 1,000 *x g* for 10 min at 4°C to pellet the cellular debris, recovering the supernatant and repeating this step. Mitochondria were pelleted by centrifuging the supernatant at 10,000 *x g* for 10 min at 4°C and washed once with isotonic buffer without BSA. Protein concentration of isolated mitochondria was determined using the Bradford assay.

### Microscopy of yeast cells

Wild-type and *tim22-14* cells transformed with the GFP-Mir1 plasmid were grown in SD-Ura media at 25°C overnight. Next day, 0.5 μM MitoTracker™ Orange CMTMRos (Thermo Fisher Scientific, MA, USA) was added to the culture. Cells were kept shaking for 20 min. Afterward, cells were harvested, washed once with media and analyzed using a DeltaVision fluorescence microscope (GE Healthcare, IL, USA). Cells grown overnight at 25°C and temperature shifted to 37°C for 25 h were treated and analyzed as above.

### Import of precursor proteins

mMessagemMachine SP6 transcription kit (Invitrogen, CA, USA) was used to generate mRNAs *in vitro* based on the manufacturer's instructions. A DNA fragment for mRNA generation was obtained by PCR using a forward primer containing a SP6 Polymerase binding site (ATTTAGGTGACACTATAG) followed by bases from the 5′ sequence of the gene and a reverse primer containing bases from the 3′ end. For synthesis of [$^{35}$S] methionine labeled protein, *in vitro* translation was carried out using the Flexi Rabbit Reticulocyte Lysate System (Promega, WI, USA). Prepared lysates were used directly for import reactions.

Import reactions were performed as previously described [31], with few modifications. Briefly, mitochondria were suspended in import buffer (250 mM sucrose, 10 mM MOPS/KOH pH 7.2, 80 mM KCl, 2 mM $KH_2PO_4$, 5 mM $MgCl_2$, 5 mM methionine and 3% fatty acid-free BSA) supplemented with 2 mM ATP, 2 mM NADH, 5 mM creatine phosphate and 0.1 mg/ml creatine kinase. For all imports into mitochondria from temperature sensitive strains, mitochondria (mutant and control) were subjected to 15 min heat shock at 37°C

prior to the import reaction. Import was performed at 25°C and terminated using AVO cocktail (final concentration 1 μM valinomyin, 8 μM antimycin A and 20 μM oligomycin) to disrupt the membrane potential. Samples were treated with 20 μg/ml Proteinase K (PK) for 10 min on ice. PK was inactivated with 2 mM phenylmethylsulphonyl fluoride (PMSF) for 10 min on ice. Mitochondria were subsequently sedimented and washed with SEM buffer. In Mpc1 and Mpc3 imports, the samples were resuspended in 100 mM sodium carbonate pH 11,5 and incubated for 30 min on ice. The membranes were sedimented at 100,000 $x$ $g$ for 1 h in TLA55 rotor. For BN-PAGE analyses of imported proteins, mitochondria were solubilized in 1.25% digitonin as described previously [42] or in 0.6% DDM for Atp5 imports. Imports into isolated human mitochondria were performed at 37°C in import buffer (250 mM sucrose, 80 mM potassium acetate, 5 mM magnesium acetate, 5 mM methionine, 10 mM sodium succinate, 5 mM adenosine triphosphate, and 20 mM HEPES/KOH pH 7.4) supplemented with 2 mM ATP, 1 mM DTT, 5 mM creatine phosphate and 0.1 mg/mL creatine kinase and 10% of radioactive lysate.

### Membrane potential measurement

Membrane potential measurements were carried out as previously described [31]. Briefly, isolated mitochondria were resuspended in potential buffer (0.6M Sorbitol, 0.1% BSA, 10 mM MgCl2, 0.5 mM EDTA, 20 mM Kpi pH 7.2) in the presence of 2mM 3,3′-Dipropylthiadicarbocyanine iodide (DISC$_3$) and changes of fluorescence (EX 622 nm/EM 670 nm) were recorded. Membrane potential was dissipated using 1mM Valinomycin. Representative images are shown, measurements were done with n = 3.

### Reduction and alkylation of proteins and tryptic digestion

Mitochondria prepared from wild-type and *tim22-14* cells harvested after 0 h, 15 h, 25 h or 40 h after temperature shift to 37°C were pelleted by centrifugation for 10 min at 12,000 $x$ $g$ and 4°C. Mitochondria were resuspended in 6 M urea dissolved in 50 mM ammonium bicarbonate. Reduction and alkylation of cysteines was performed as described before [43]. Samples were diluted with H$_2$O to a final urea concentration of 1.5 M. Sequencing grade trypsin (Serva, Heidelberg, Germany) was added in a 1:30 (trypsin:protein) ratio and samples were incubated at 37°C overnight. Tryptic digests were acidified by adding trifluoroacetic acid (TFA) to a final concentration of 0.7% (v/v).

### Dimethyl labeling of peptides on StageTips

StageTips were assembled as described previously [44] using three discs of C18 material (Empore 3M) per tip. StageTips were conditioned with 25 μl of 100% methanol, equilibrated with 25 μl of 0.5% (v/v) acetic acid/80% (v/v) acetonitrile (ACN) and washed twice with 25 μl of 100 mM triethylammonium bicarbonate (TEAB), each by centrifugation at 800 $x$ $g$ for 1-2 min. 10 μg of acidified peptides were loaded onto each StageTip by centrifugation at 800 $x$ $g$ for 5 min. Labeling solutions were freshly prepared by mixing 70 μl of 50 mM monosodium phosphate with 245 μl of 50 mM disodium phosphate, 17.5 μl of 4% (v/v) formaldehyde in 100 mM TEAB and 17.5 μl of 0.6 M sodium cyanoborohydride in 100 mM TEAB. For labeling of peptides from wild-type cells, the light versions of formaldehyde and sodium cyanoborohydride (CH$_2$O and NaBH$_3$CN, Sigma-Aldrich) were used. For peptides from *tim22-14* control cells (grown at 25°C), deuterated formaldehyde (CD$_2$O, Sigma-Aldrich) and light NaBH$_3$CN were mixed. For peptides from *tim22-14* cells harvested 15 h, 25 h or 40 h after shift to 37°C, deuterated $^{13}$C-labeled formaldehyde ($^{13}$CD$_2$O, Sigma-Aldrich) and deuterated sodium cyanoborohydride (NaBD$_3$CN; Sigma-Aldrich, MO, USA) were used. For labeling, StageTips were loaded twice with 150 μl of the respective labeling solution and centrifugation at 800 $x$ $g$ for 5-7 min. StageTips were washed twice with 25 μl of 100 mM TEAB. Peptides were eluted twice with 20 μl of 0.5% (v/v) acetic acid/80%(v/v) ACN by centrifugation at 800 $x$ $g$ for 1 min. Light-, medium- and heavy-labeled samples were mixed and dried *in vacuo*.

### Desalting and fractionation of samples

StageTips were assembled as described previously [44] using three discs of C18 material (Empore 3M) per tip for each 17 to 20 μg of mixed peptides. StageTips were conditioned and equilibrated as described above and washed twice with 25 μl of 0.5% (v/v) acetic acid. Dried peptides were resuspended in 50 μl of 0.5% (v/v) acetic acid and loaded onto the StageTips by centrifugation at 800 $x$ $g$ for 2-5 min. StageTips were washed twice with 25 μl of 0.5% (v/v) acetic acid. Each sample was fractionated in eight fractions by sequential basic elution using 20 μl of 10 mM ammonium hydroxide (pH 10) with increasing concentrations of ACN (i.e., 0%, 2.7%, 5.4%, 9%, 11.7%, 14.4%, 22.5% and 64.8%; v/v each). Peptides were dried *in vacuo* and resuspended in 20 μl of 0.1%(v/v) TFA, of which 15 μl were used for LC-MS/MS analysis.

### LC-MS analysis

Nano-HPLC-ESI-MS/MS analyses were performed on an Orbitrap Elite mass spectrometer (Thermo Fisher Scientific, MA, USA) connected to an UltiMate 3000 RSLCnano HPLC system (Thermo Fisher Scientific, MA, USA). Samples were washed and preconcentrated using C18 precolumns (nanoEase™ M/Z Symmetry C18; length, 20 mm; inner diameter, 180 μm; Waters) with a flow rate of 5 μl/min for 5 min. Peptide separation was performed using a C18 reversed-phase nano LC column (nanoEase™ M/Z HSS C18 T3; length, 25 cm; inner diameter, 75 μm; particle size, 1.8 μm; pore size, 100 Å; Waters) at 40°C and a flow rate of 300 nl/min. Peptides were separated using a binary solvent system consisting of 0.1% (v/v) FA/4% (v/v) dimethyl sulfoxide (DMSO) (solvent A) and 48% methanol/30% ACN/0.1% (v/v) FA/4% (v/v) DMSO (solvent B). They were eluted with a gradient of 5%–65% B in 65 min and 65%–80% B in 5 min. Subsequently, the analytical column was washed with 80% B for 5 min before re-equilibration with 100% A. Peptides eluting from the column were transferred to a fused silica picotip emitter (SilicaTip™, NewObjective) via a DirectJunction™ adaptor

(Thermo Fisher Scientific) for electrospray ionisation (ESI, source voltage 1.5-1.8 kV, temperature of heated capillary 200°C) using a nanospray flex ion source (Thermo Fisher Scientific). Mass spectra were acquired in a mass-to-charge (m/z) range of 370-1,700 with a resolution (R) of 120,000 at m/z 400. Automatic gain control (AGC) was set to $1 \times 10^6$ with a maximum (max.) injection time of 200 ms. The 25 most intense peptide ions were selected for low-energy collision-induced dissociation experiments in the linear ion trap with the following parameters: normalized collision energy, 35%; activation q, 0.25; activation time, 10 ms; AGC, 5,000; max. injection time, 150 ms; isolation width, m/z 2.0. The instrument was operated in the positive ion mode for data-dependent acquisition of MS/MS spectra. The dynamic exclusion time of previously selected precursor ions was set to 45 s and only +2 or higher charged ions were selected for MS/MS fragmentation.

### MS data analysis
Raw files of LC-MS/MS analyses were jointly processed using MaxQuant v.1.6.0.1 [45]. For peptide identification, spectra were correlated with the *Saccharomyces cerevisiae* protein database (UniProtKB canonical set including isoforms for strain AC204508/S288c, Proteome ID UP000002311, release 01.02.2018, 6,757 entries) using Andromeda [46]. N-terminal and lysine dimethylation were set as light (+28.03 Da), medium (+32.06 Da) and heavy (+36.08 Da) labels, respectively. Trypsin was set as the enzyme in specific digestion mode allowing two missed cleavage sites. Oxidation of methionine was included as variable modification and cysteine carbamidomethylation was set as fixed modification. The minimum peptide length was set to 6 amino acids. The precursor mass tolerance was set to 20 ppm for the "first search" option of Andromeda and to 4.5 ppm for the main search. MSMS match tolerance was set to 0.5 Da. A false discovery rate of 1% was applied to both peptide and protein lists using the decoy mode "Revert." For protein quantification, the option "Re-quantify" was checked and the option "Match between runs" was enabled with a retention time window of 0.7 min. The minimum ratio count for protein quantification was set to two and only unique peptides were considered for protein quantification. Normalized heavy-over-light ratios of the MaxQuant output file "proteingroups."txt (excluding entries marked as contaminants, 'reverse' and 'only identified by site') were log-transformed. Light and heavy intensities for each protein group were summed up and log-transformed. Mean $\log_2$ ratios and mean $\log_2$ intensities were calculated across the treated samples (15 h, 25 h and 40 h after temperature shift to 37°C). Perseus v.1.5.5.3 [47] was used to determine significant outliers in the different populations with the implemented algorithm "Significance B," setting a P value significance threshold to 0.05. Proteins or protein groups were annotated as "mitochondrial carrier protein" if the protein or at least one protein of the group was part of the high-confidence mitochondrial proteome [48] and contained the term "carrier" in its protein description.

### QUANTIFICATION AND STATISTICAL ANALYSIS

For steady-state analysis of proteins, quantifications were performed from the corresponding immunoblots using ImageQuant TL (GE Healthcare, NJ, USA) using a rolling ball background subtraction.

For analysis of imports, after digital autoradiography, quantifications were performed using ImageJ. A threshold was applied to select the area of interest and minimize non-specific signal. Integral intensities of these areas were acquired. For yeast, time points in the linear range of import reaction were considered.

### DATA AND CODE AVAILABILITY

The proteomic dataset generated in this study is included as Table S1 associated with this manuscript.